Simulating Shear Thickening Flow in 2D Channel

Morten Vester Pedersen
mvp288@nyu.edu

December 31, 2016

A nonlinear Stokes equation is studied in preparation for simulation of free falling in shear thickening fluids. A shear thickening fluid is a non-Newtonian fluid in which particles are suspended at a high particle-to-fluid volume fraction. At high strain rates, the particles are pushed closely together resulting in an increase of the viscosity. The non-Newtonian fluid dynamics are modeled using a nonlinear Stokes equation. The PDE is formulated in a mixed variational form, which is discretized using finite elements. A Newton Descent method is implemented with backtracking line-search to solve the an equivalent minimization problem utilizing the variational form. Results are presented and an outline for future work is given.

1 Introduction

The physical behavior of shear thickening fluids, or dilatants, are seen in a variety of materials. A well know dilatant is oobleck, a mixture of cornstarch and water. It has been popularized in online videos that shows the dramatic properties of the fluid. An example is, if the mixture is stirred slowly is looks and feels much like milk. However, when stirred faster, i.e. under higher strain rate, the mixture becomes more viscous and feels more like a thick yogurt. Other, more common, materials also include paint, cements and clays.

In some cases, the non-Newtonian behavior of dilatant sought-for property that can be utilized for shock absorbance or in fluid-filled dampers for seismic protection of buildings [7]. However it is not always a sought for property. In spraying equipment, the increase in viscosity can cause severe problems. If the fluid becomes too viscous it could potentially ruin the equipment due to congestion.

In this study, the fluid is modeled using a similar rheology of that used in simulations of ice sheet dynamics [3]. However, ice sheet simulations rely on shear thinning, i.e. the fluid becomes less viscous. Mathematically speaking the behavior is described by the same equation with the difference coming from a choice of exponent.

The end goal is to simulate a free falling object in a shear thickening fluid. In [6] it was shown that the velocity of a free falling sphere oscillates due to the changing viscosity. Furthermore, at times the sphere came to a complete halt before returning to it's descent towards the bottom of the container. Simulating the two-way coupled interaction of fluid and

solid has, to the best of my knowledge, not been done before and is rather valuable due to applicability of dilatant in industry. Thus the goal is to simulate this behavior to produce a good mathematical model for shear thickening fluids.

In the following pages, a theoretical foundation is built. Starting from a nonlinear Stokes equation with the thickening having polynomial dependence on the strain rate. The PDE has an equivalent energy minimization problem formulation from which variations are taken. The variations are then discretized and the minimization problem is solved using a Newton descent algorithm. Experiments on a geometrically simple domain are presented and an outline of future work is given.

2 Problem Formulation

The basis of this study is a nonlinear Stokes Equation. Given a domain $\Omega \subset \mathbb{R}^2$, the fluid is modeled as a non-Newtonian, viscous, incompressible fluid given by

$$-\nabla \cdot \sigma = f \quad \text{in } \Omega \tag{1a}$$
$$\nabla \cdot u = 0 \quad \text{in } \Omega \tag{1b}$$

Here u is the velocity vector, f is a external forcing and σ is the stress tensor. Furthermore, a mapping $\mathcal{E}$ from velocity to shear strain rate is given by

$$\mathcal{E}u = \frac{1}{2}(\nabla u + \nabla u^T), \qquad |\mathcal{E}u| = (\mathcal{E}u : \mathcal{E}u)^{1/2} \tag{1c}$$

where " : " denotes the inner product of two second order tensors, i.e. $A : B = \sum_{i,j} A_{i,j} B_{i,j}$. Depending on the problem of interest the stress tensor σ can defined differently. One example, where the increase in viscosity is sudden, is given in [5]. As in [3], we define the stress tensor σ such that it depends continuously on the shear strain rate

$$\sigma = -pI + \mu \left|\mathcal{E}u\right|^{\frac{1-n}{n}} \mathcal{E}u \tag{1d}$$

In **Eqn (1d)**, p denotes pressure and μ is the viscosity parameter. n is strain rate exponent and for $n = 1$, **Eqn (1d)** reduces to linear rheology, while for $n < 1$ the equation describes a shear thickening fluid.

The domain of interest in this study, has been restricted to a $2D$ channel with an obstacle inside. Physically the domain represent a channel of infinite depth with a cylindrical obstacle in the middle. In **Figure 1** the domain is sketched along the mixed boundary conditions as described in **Eqn (2)**

$$u = 0 \qquad \text{on } \Gamma_T \cup \Gamma_B \cup \Gamma_C \tag{2a}$$
$$u = -x_2^2 + x_2 \qquad \text{on } \Gamma_I \tag{2b}$$
$$\nabla u \cdot n = 0 \qquad \text{on } \Gamma_O \tag{2c}$$

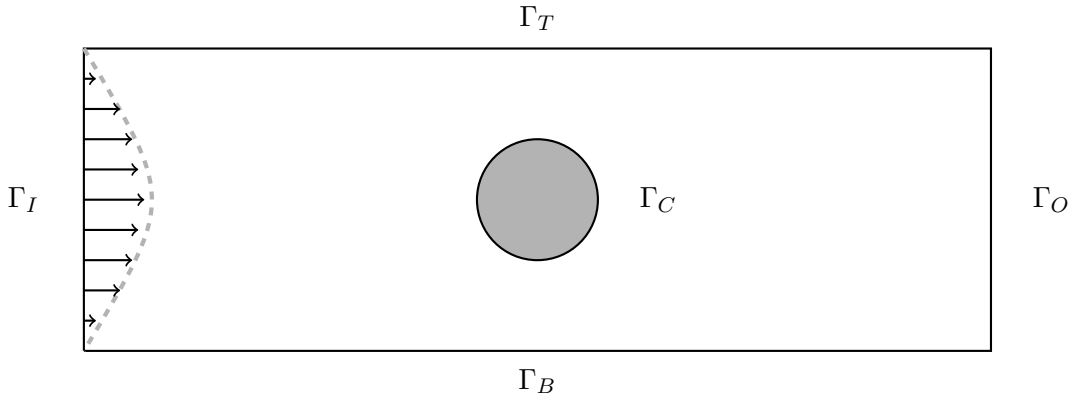

Figure 1: Domain for interest, $\Omega = ([0,3] \times [0,1]) \backslash B([1.5,.5],.20)$

3 Variational Form and Discretization

In the following, **Eqn (1)** is formulated in a mixed variational form and it is shown that a solution to **Eqn (1a)** also is the minimizer of a corresponding minimization problem. A Newton linearization is derived and discrete versions are presented.

For simplicity of notation, we define u_0, a function that satisfies the boundary conditions of **Eqn (2)**. Three function spaces are defined

$$\begin{aligned} \mathcal{V} &= \left\{ u \in H^1(\Omega) \middle| \nabla \cdot u = 0,\ u = u_0 \text{ on } \partial\Omega \right\} \\ \mathcal{V}_0 &= \left\{ u \in H^1(\Omega) \middle| \nabla \cdot u = 0,\ u = 0 \text{ on } \partial\Omega \right\} \\ \mathcal{P} &= L_2(\Omega) \end{aligned}$$

Where $H^1(\Omega)$ is a Hilbert-Sobolev space [1, p. 261]. The energy minimization problem is given by [3]

$$\min_{(u,p)\in\mathcal{V}\times\mathcal{P}} J(u,p) = \mu \frac{n}{n+1} \int_\Omega |\mathcal{E}u|^{\frac{1+n}{n}}\ dx - \int_\Omega f \cdot u + p\nabla \cdot u\, dx \tag{3}$$

Notice that the last term $p\nabla \cdot u = 0$ due to u being a divergence free function. However, it serves a purpose in deriving variations and it is left in for that reason. A minimizer (u^*, p^*) must necessarily satisfy

$$J(u^*, p^*) \leq J(u^* + \delta v, p^* + \delta q), \quad \forall (v,q) \in \mathcal{V}_0 \times \mathcal{P}$$

See that

$$\begin{aligned} J(u^* + \delta v, p^* + \delta q) =& \mu \frac{n}{n+1} \int_\Omega |\mathcal{E}(u^* + \delta v)|^{\frac{1+n}{n}}\ dx \\ & - \int_\Omega f \cdot (u^* + \delta v) + (p^* + \delta q)\nabla \cdot (u^* + \delta q)\, dx \end{aligned} \tag{4}$$

The derivative with respect to δ is

$$\frac{\partial J(u^* + \delta v, p^* + \delta q)}{\partial \delta} = \mu \int_\Omega |\mathcal{E}(u^* + \delta v)|^{\frac{1-n}{n}} \left[(\mathcal{E}u^* : \mathcal{E}v) + \delta(\mathcal{E}v : \mathcal{E}v) \right] dx - \int_\Omega f \cdot v \, dx + \int_\Omega p^* \nabla \cdot v + q \nabla \cdot u^* + 2\delta q \nabla \cdot v \, dx \tag{5}$$

Which for $\delta = 0$ reduces to

$$\delta J(u^*, p^*)(v, q) = \mu \int_\Omega |\mathcal{E}u^*|^{\frac{1-n}{n}} (\mathcal{E}u : \mathcal{E}v) \, dx - \int_\Omega f \cdot v + p^* \nabla \cdot v + q \nabla \cdot u^* \, dx = 0 \tag{6}$$

Using integration by parts in conjunction with the divergence theorem, cf. **Eqn (18)**, on the first term yields

$$\delta J(u^*, p^*)(v, q) = \mu \int_\Omega -\nabla \cdot (|\mathcal{E}u^*|^{\frac{1-n}{n}} \mathcal{E}u) v \, dx - \int_\Omega f \cdot v + p^* \nabla \cdot v + q \nabla \cdot u^* \, dx + \int_{\partial\Omega} |\mathcal{E}u^*|^{\frac{1-n}{n}} \mathcal{E}u^* \cdot n \, ds \tag{7}$$

or equivalently

$$\int_\Omega \left[-\mu \nabla \cdot (|\mathcal{E}u^*|^{\frac{1-n}{n}} \mathcal{E}u + p^* I) - f \right] v \, dx - \int_\Omega q \nabla \cdot u^* \, dx + \int_{\partial\Omega} |\mathcal{E}u^*|^{\frac{1-n}{n}} \mathcal{E}u^* \cdot n \, ds = 0 \tag{8}$$

Notice that **Eqn (8)** must be equal to zero for all $(v, q) \in \mathcal{V}_0 \times \mathcal{P}$. This only happens if (u^*, p^*) satisfy **Eqn (1)** with the boundary conditions found in **Eqn (2)**. Thus it has been seen that the nonlinear Stokes equation matches the minimization problem given in **Eqn (3)**.

The first variation found in **Eqn (6)** defines a Picard Linearization of the minimization problem. To obtain a Newton linearization a second variation is taken, starting from **Eqn (6)**

$$\delta^2 J(u, p)((v, q), (w, r)) = \mu \frac{1-n}{n} \int_\Omega |\mathcal{E}u|^{\frac{1-3n}{n}} (\mathcal{E}u : \mathcal{E}w)(\mathcal{E}u : \mathcal{E}v) \, dx + \mu \int_\Omega |\mathcal{E}u|^{\frac{1-n}{n}} (\mathcal{E}v : \mathcal{E}w) \, dx + \int_\Omega r \nabla \cdot v + q \nabla \cdot w \, dx \tag{9}$$

Similarly as in [3] a Newton linearization is established using **Eqn (6)** and **Eqn (9)** given by

$$\delta^2 J(u, p)((v, q), (w, r)) = -\delta J(u, p)(v, q) \tag{10}$$

Given a pair (u, p), **Eqn (10)** is solved for the search direction (w, r).

3.1 Discretization

For discretization, finite-element spaces are introduced. $V_h \subset H^1(\Omega) is for the velocity$ and $P_h \subset L_2(\Omega)$ for the pressure. Following the steps of [2] the functions of **Eqn (6)** are replaced with discrete versions leading to

$$\mu \int_\Omega |\mathcal{E}u_h|^{\frac{1-n}{n}} (\mathcal{E}u_h : \mathcal{E}v_h)\, dx - \int_\Omega p_h \nabla \cdot v_h = \int_\Omega f_h \cdot v_h \qquad \forall v_h \in V_h \tag{11a}$$

$$q_h \nabla \cdot u_h\, dx = 0 \qquad \forall q_h \in P_h \tag{11b}$$

Using numerical quadrature for the integrals above and denoting the finite element coefficients of functions (u_h, p_h) by $(\bar{\boldsymbol{u}}, \bar{\boldsymbol{p}})$, **Eqn (11a)** is rewritten

$$\begin{pmatrix} \mathbf{A}(\bar{\boldsymbol{u}}) & \mathbf{B}^T \\ \mathbf{B} & \mathbf{0} \end{pmatrix} \begin{pmatrix} \bar{\boldsymbol{u}} \\ \bar{\boldsymbol{p}} \end{pmatrix} = \begin{pmatrix} \boldsymbol{f} \\ \mathbf{0} \end{pmatrix} \tag{12}$$

Here $\mathbf{A}(\bar{\boldsymbol{u}})$ is the discretization of the viscous term corresponding to the first term in **Eqn (11a)** and $\mathbf{B}$ is the discrete divergence operator. The discrete version for the right hand side in **Eqn (10)** is

$$\begin{pmatrix} \boldsymbol{f} - \mathbf{A}(\bar{\boldsymbol{u}}) - \mathbf{B}^T \bar{\boldsymbol{p}} \\ \mathbf{0} \end{pmatrix} \tag{13}$$

Notice that $\bar{\boldsymbol{u}}$ is divergence free thus the second term is set to zero, enforcing this property. The second variation is discretized in a similar manner yielding the following Newton system from which the search direction $(\hat{\mathbf{u}}, \hat{\mathbf{p}})$ is obtained. At iteration k, $(\bar{\boldsymbol{u}}_k, \bar{\boldsymbol{p}}_k)$ is given and the search direction is found from

$$\begin{pmatrix} \tilde{\mathbf{A}}(\bar{\boldsymbol{u}}_k) & \mathbf{B}^T \\ \mathbf{B} & \mathbf{0} \end{pmatrix} \begin{pmatrix} \hat{\mathbf{u}} \\ \hat{\mathbf{p}} \end{pmatrix} = \begin{pmatrix} \boldsymbol{f} - \mathbf{A}(\bar{\boldsymbol{u}}_k) - \mathbf{B}^T \bar{\boldsymbol{p}}_k \\ \mathbf{0} \end{pmatrix} \tag{14}$$

Here $\tilde{\mathbf{A}}$ is the discretization of the two nonlinear terms involving μ in **Eqn (9)**.

3.2 Newton descent

A simple Newton descent with Armijo backtracking line search is used. The iterates are given by

$$(\bar{\boldsymbol{u}}_{k+1}, \bar{\boldsymbol{u}}_{k+1}) = (\bar{\boldsymbol{u}}_k, \bar{\boldsymbol{p}}_k) + \alpha(\hat{\mathbf{u}}, \hat{\mathbf{p}}) \tag{15}$$

Where $\boldsymbol{\alpha}$ is the step size. The Armijo condition is

$$J(\bar{\boldsymbol{u}}_k + \alpha\hat{\mathbf{u}}, \bar{\boldsymbol{p}}_k + \alpha\hat{\mathbf{p}}) < J(\bar{\boldsymbol{u}}_k, \bar{\boldsymbol{p}}_k) + \alpha\eta\, \boldsymbol{M}_k \tag{16}$$

With η being the Armijo coefficient and $\boldsymbol{M}_k$ denoting the inner product of the first variation and the search direction given by

$$\boldsymbol{M}_k = \begin{pmatrix} \hat{\mathbf{u}} & \hat{\mathbf{p}} \end{pmatrix} \begin{pmatrix} \boldsymbol{f} - \mathbf{A}(\bar{\boldsymbol{u}}_k) - \mathbf{B}^T \bar{\boldsymbol{p}}_k \\ \mathbf{0} \end{pmatrix} \tag{17}$$

4 Experiments and Results

Following is a short introduction of experiments, an analysis of the Newton method and the obtained solution. In all experiments, the viscosity parameter $\mu = 1$ and the forcing $f = 0$. The backtracking line search is also implemented with the widely used values of $\eta = 10^{-4}$ and $\gamma = 1/2$, where γ is the reduction factor. The experiment of flow through a channel with an obstacle, as sketched in **Figure 1**, is repeated several times for different strain rate exponents n between $[1/4, 5]$ and on meshes of different resolution.

To begin, the variational expressions are verified through finite difference. The error, or difference as seen in **Figure 2**, is defined as the difference in directional derivatives. One is computed through first order finite difference and the other through the variations. Notice that for both the gradient and Hessian expressions, the decrease is of first order, as expected due to the choice of finite difference scheme.

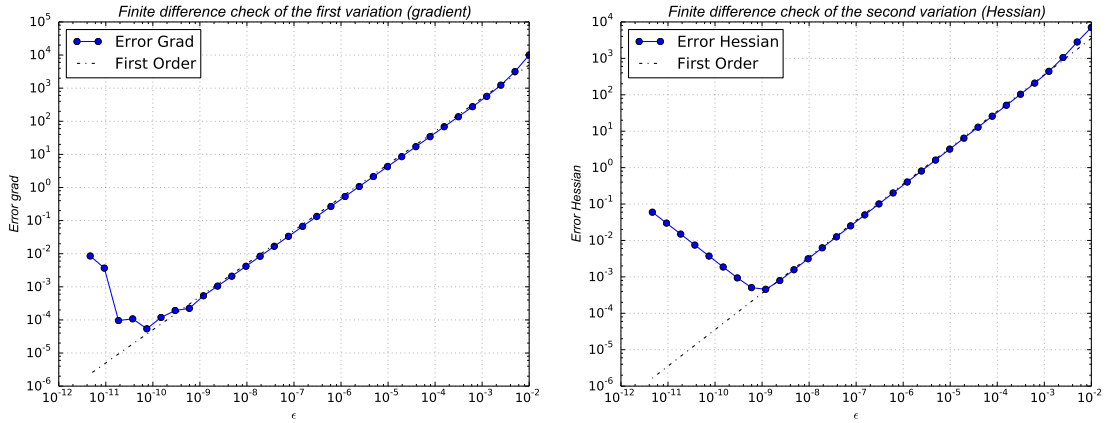

(a) (b)

Figure 2: Verification of variational expressions through finite difference of the gradient(left) and Hessian(right) expressions.

ele dof	3646 16921	14605 66744	32718 149040	58088 263450	89491 405231
$n = 0.25$	16	15	16	19	21
$n = 0.50$	7	7	7	7	8
$n = 2.0$	9	12	15	15	17

Table 1: Results concerning mesh refinement. The discrete mesh coarseness is defined by the number of finite elements and degrees of freedom in the corresponding Stokes system.

In **Table 1**, results concerning refinement of the mesh discretization is presented for different strain rate parameters. It is seen that the number of iterations is largely independent of the mesh. The largest factor seems to the the strain rate parameter. Not surprisingly, since this is the source of the nonlinearity. The Newton linearizion is a good approximation for strain

rate parameters close to $n = 1$, i.e. the linear Stokes problem, by for stronger non-linearities it becomes less accurate. Nonetheless, the increase in the number of required iterations is fairly modest in all cases, compared in the increase of unknowns(degrees of freedom).

n	iter	time	$J(u)$	(g_k, d_k)	$\|\|g_k\|\|$	#non-unit steps
0.25	16	89.936743	2.533820e+00	-1.801629e-15	5.823987e-09	2
0.5	7	35.510017	1.033414e+00	-3.401586e-15	8.015426e-08	0
0.75	5	26.241054	9.310875e-01	-5.114125e-23	1.026535e-11	0
2.0	15	81.125891	1.077032e+00	-6.214568e-20	1.832605e-09	0
3.0	18	96.942566	1.162294e+00	-1.610990e-19	7.517352e-09	6
5.0	24	139.854741	1.247944e+00	-1.314893e-15	2.054432e-06	16

Table 2: Experiments Summary. The domain consists of 32718 finite elements with a total of 149040 degrees of freedom.

In **Table 2** a summary of each experiment is seen. Here all experiments had the mesh, consisting of 32718 finite elements with 149040 degrees of freedom. Generally, as the strain rate exponent n increases or decreases away from the linear case of $n = 1$, the number of iterations required in the Newton method increases. For "strong" nonlinearities, e.g. $n = 5$ it is noticed that over half of the iterations, the method cannot take a unit step. This is expected to kill the usual fast convergence of the Newton method.

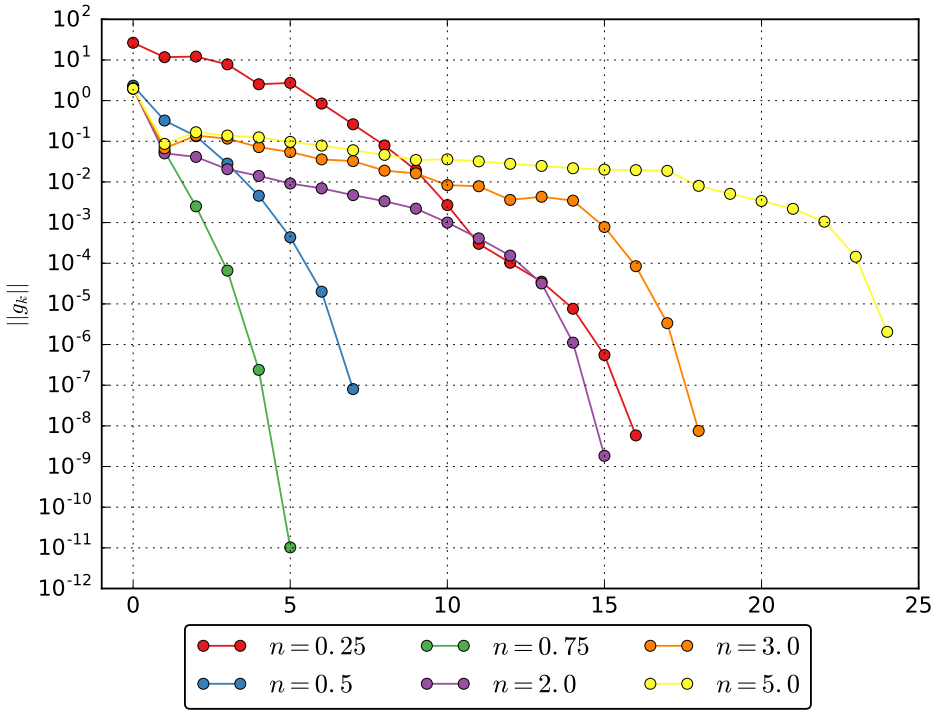

Figure 3: Convergence plot for different strain rate exponents, showing the norm of the gradient on a log scale with respect the the iteration number.

In **Figure 3** a log-plot of the norm of the gradient expression is seen. In All cases, the fast convergence seems to kick in when sufficiently close the the solution, as expected for a Newton descent method. Also, for strong nonlinearities, e.g. $n = 3$ or $n = 5$, not much progress is made in the first iterations 10-15 iterations, where the descent method often took a non-unit step.
Having considered the behavior of the variational expressions and Newton descent method, the focus turns to the solutions obtained. First we consider solutions near the inflow boundary.

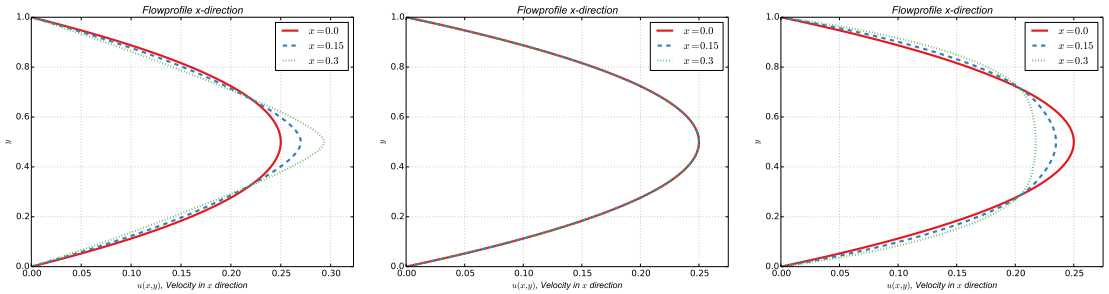

Figure 4: Flow profile in the x direction at and close to the inflow boundary. From left to right, the strain rate exponents are $0.25,\ 1,\ 5.0$. In all three plots the red line shows the flow profile at the boundary, i.e. $x = 0$, and is therefore equal to the boundary condition. The two other lines show the flow profile at $x = 0.15$ and $x = 0.3$.

In **Figure 4b** the flow profile of a linear stokes equation is shown. Here, we notice that the flow profile does not change when moving away from the inflow boundary. If the domain was a channel with no obstacle this profile would continue through the domain, only the obstacle changes the flow profile.
In the shear thickening case, $n = 0.5$, seen in **Figure 4a**, we notice that the flow profile changes as you move away from the boundary. The fluid is thickened near the top and bottom boundaries, pushing the fluid towards the center of the channel, accelerating the flow and thereby stretching the flow profile. In **Figure 4c**, the flow profile of a thinning experiment is seen. Again the flow profile is deformed compared to the inflow boundary, when moving away from the boundary. This time the flow profile is squashed, slowing the flow in the center of the channel, but slightly accelerating the flow closer to the top and bottom boundaries.
This behavior is expected and qualitatively they are identical to that seen in [4, p. 96]. Note that even though the flow profile are qualitatively different comparing shear thickening fluid to linear stokes model, due to having the same boundary conditions, the overall flow of the whole domain is the same. Only the qualitative behavior of the flow changes.

Comparing the flow of shear thickening fluids to that of linear Stokes flow, **Figure 5** shows the streamlines of three different solutions. It can be observed that the streamlines concentrate further away from the boundaries compared to a linear flow. This behavior aligns with the findings for [5].

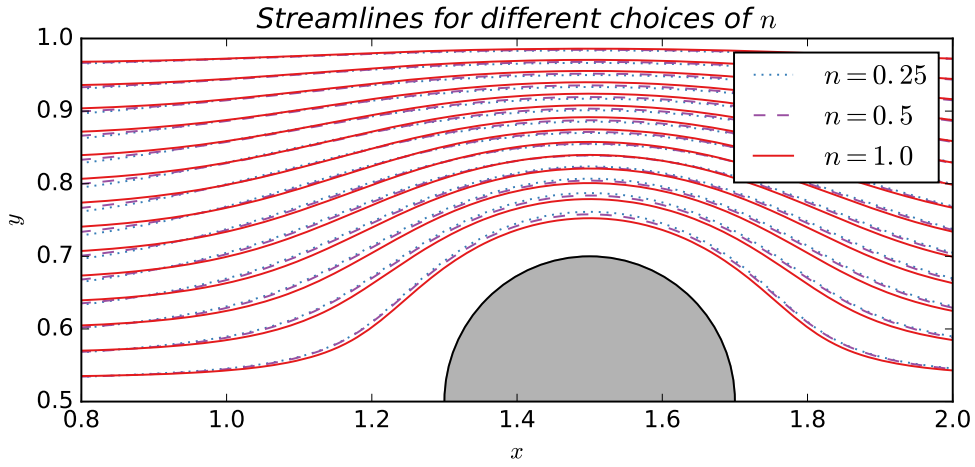

Figure 5: Streamlines in the upper half of the domain. Shown are streamlines for different strain rate parameters, qualitatively showing the difference between a linear Stokes flow and that of a shear thickening fluid.

In **Figure 6** a plot of the thickening of the fluid is shown. Observe that the thickening concentrates close to the obstacle, but also occurs at the top boundary. Due to the shear thickening being smooth, no free boundary arises as in [5]. However the geometrical shape of the thickened volume is similar to what was found in [5]. Considering the thickened volume depending on the strain rate parameter, the qualitative behavior seem to be independent of n. The shape of the thickened volume is similar in the two cases presented in **Figure 6**. However, there is a dramatic difference in the intensity of the thickening. For smaller strain rate parameters, the thickening is much stronger.

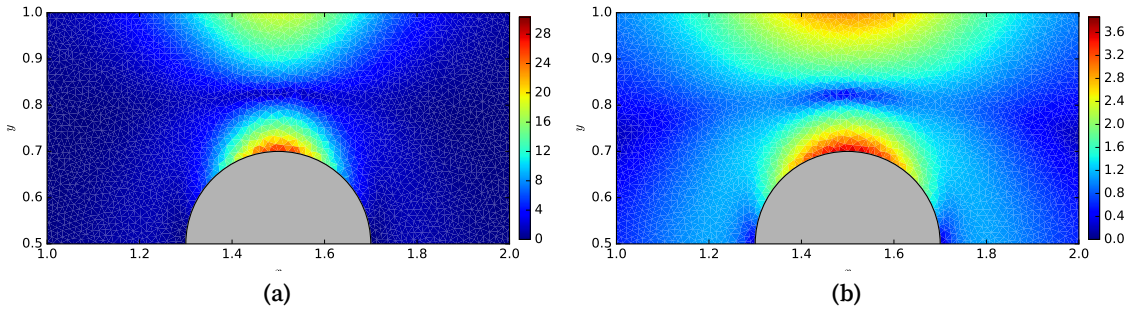

Figure 6: Thickening of the fluid in the upper half of the channel centered on the obstacle. In **Figure 6a** the strain rate parameter is $n = 0.25$, while in **Figure 6b** it is $n = 0.5$.

5 Conclusion and Future Work

As mentioned in the beginning, the goal is to simulate a free falling object in a shear thickening fluid. With this work the foundation has been built, through a Newton Descent method that solves a nonlinear Stokes problem. The current solution algorithm has been seen to

work well for a varity of strain rate exponents. The Newton method behaves in the usual manner, often taking small steps in the first couple of iterations and showing fast convergence close the the solution. Furthermore, from the flowprofiles and streamlines, the solutions have been seen to be consistent with that of previous findings.
To simulate a free falling object, a series of stokes flow problems will be solved. After each solution the forces enacted on the object must be calculated and adapting the boundary to infer the movement of the sphere. Furthermore, extending this work from a 2D domain to a 3D is also on the horizon. The biggest challenge here, is the solution of a Newton system. It is highly likely that an iterative solver must be used and therefore some work will go in to finding a good preconditioner and iterative method.

6 Appendix

Multidimensional Integration by Parts using the divergence theorem

$$\int_\Omega \nabla \cdot (k\nabla u)v \, dx = \int_{\partial\Omega} k(\nabla u \cdot n)v \, ds - \int_\Omega k(\nabla u \cdot \nabla v) \, dx \tag{18}$$

Code Output

References

[1] Haim Brezis. Functional analysis, Sobolev spaces and partial differential equations. Springer Science & Business Media, 2010.

[2] Howard C Elman, David J Silvester, and Andrew J Wathen. Finite elements and fast iterative solvers: with applications in incompressible fluid dynamics. Oxford University Press (UK), 2014.

[3] Tobin Isaac, Georg Stadler, and Omar Ghattas. Solution of nonlinear stokes equations discretized by high-order finite elements on nonconforming and anisotropic meshes, with application to ice sheet dynamics. SIAM Journal on Scientific Computing, 37(6): B804–B833, 2015.

[4] Martin J Rhodes. Introduction to particle technology. John Wiley & Sons, 2008.

[5] Georg Stadler. A nonsmooth model for discontinuous shear thickening fluids: analysis and numerical solution. Interfaces and Free Boundaries, 16:575–602, 2014.

[6] Stefan von Kann, Jacco H. Snoeijer, Detlef Lohse, and Devaraj van der Meer. Nonmonotonic settling of a sphere in a cornstarch suspension. Phys. Rev. E, 84:060401, Dec 2011.

[7] XZ Zhang, WH Li, and XL Gong. The rheology of shear thickening fluid (stf) and the dynamic performance of an stf-filled damper. Smart Materials and Structures, 17(3): 035027, 2008.